Nanoscale Horizons

ROYAL SOCIETY OF CHEMISTRY

COMMUNICATION

View Article Online
View Journal | View Issue

Cite this: *Nanoscale Horiz.*, 2024, 9, 2051

Received 18th June 2024,
Accepted 29th August 2024

DOI: 10.1039/d4nh00285g

rsc.li/nanoscale-horizons

Durable silver nanowire transparent electrodes enabled by biorenewable nanocoating using chitin and cellulose nanofibers for flexible electronics†

Yoo-Bin Kwon,[a] Seongwon Cho,[b] Dal-Hee Min *[a] and Young-Kwan Kim *[b]

The protection of silver nanowire (AgNW) networks is crucial for enhancing their durability and applicability to flexible electronics. In this study, we present a sustainable and efficient strategy to protect AgNW-based flexible transparent electrodes (FTEs) using a layer-by-layer (LBL) assembly of biorenewable chitin and cellulose nanofibers (Chi and Cell). These uniform LBL-assembled thin films were successfully fabricated on AgNW FTEs due to their opposite surface charges. The resulting (Chi/Cell)$_n$ bilayers, where *n* is the number of bilayers, did not degrade the optoelectrical properties of AgNW FTEs and significantly enhanced their stability under various harsh conditions. The optimized (Chi/Cell)$_{10}$@Al-AgNW FTEs exhibited comprehensive stability against UV/O_3 treatment for 40 min, thermal treatment at 250 °C for 350 min, Na_2S (1%), HCl (10%), and NH_3 (30%) treatments for 3, 30, and 105 min, respectively, sonication for 300 min, and 10 000 cycles of bending test. Therefore, the (Chi/Cell)$_{10}$@Al-AgNW FTEs were successfully applied to transparent heaters (TH) and pressure sensors with remarkably improved applicability, durability, and performance compared to pristine AgNW FTEs, providing a reassuring solution to the stability issues of AgNW-based FTEs.

New concepts

The application of silver nanowire (AgNW)-based flexible transparent electrodes (FTEs) to flexible electronics has been limited by their low optical, oxidation, thermal, chemical, and mechanical stability. To enhance the stability of AgNW FTEs using an eco-friendly strategy, biorenewable thin films composed of chitin and cellulose nanofibers (Chi and Cell) are fabricated on AgNW FTEs through the layer-by-layer (LBL) assembly process to harness their excellent transparency, flexibility, mechanical and gas barrier properties. The thin films of Chi and Cell are explored for the first time as protective coating layers for AgNW FTEs. Their optimized thin films not only significantly improve the comprehensive stability of AgNW FTEs but also their performance as transparent heaters and pressure sensors. Our new concept will considerably facilitate the development of flexible electronic devices using AgNW-based FTEs.

Introduction

Flexible transparent electrodes (FTEs) are essential components of flexible electronic devices such as touch screens, smart windows, thin-film solar cells, transparent heaters, organic light-emitting diodes, memory devices, transistors, *etc.*[1–11] The use of indium tin oxide (ITO) as a primary material to fabricate transparent electrodes has been widespread, but this traditional material poses significant challenges for FTEs due to its intrinsic brittleness, resource scarcity, and complicated fabrication process.[12–14] Hence, considerable research has been dedicated to finding alternatives to ITO, leading to the use of various nanomaterials such as metallic nanowires (NW), carbon nanotubes (CNT), graphene, and MXene for flexible electronics.[15–18] Among these, silver NWs (AgNWs) have emerged as promising materials, thanks to their excellent flexibility, transparency, solution processability, and electrical conductivity.[19–22] However, the practical applications of AgNW-based FTEs have been hindered by their low oxidation, thermal, chemical, and mechanical stability, which is attributed to the high surface energy of AgNWs and their poor adhesion to substrates.[23–25]

Diverse protection strategies have been developed to improve the stability of AgNWs, and the most efficient approach is coating the surface of AgNWs with highly stable and integrative thin films composed of graphene derivatives,[26–28] metal/metal oxides,[29–31] polymers,[32–34] or thiol ligands.[35–37] Although these

[a] *Department of Chemistry, Seoul National University, Seoul 08826, Republic of Korea. E-mail: dalheemin@snu.ac.kr*
[b] *Department of Chemistry, Dongguk University, 30 Pildong-ro, Jung-gu, Seoul, 04620, Republic of Korea. E-mail: kimyk@dongguk.edu*

† Electronic supplementary information (ESI) available: Characterization of AgNWs, Chi, and Cell, diameter histograms of (Chi/Cell)$_n$@Al-AgNW TEs, C 1s XPS spectra of Al-AgNW and Chi@Al-AgNW TEs, SEM images of AgNW and (Chi/Cell)$_{10}$@Al-AgNW TEs after UV/O_3 treatment, heat treatment, and applying 10 V. Schematic diagram of the method for chemical stability tests, temperature profiles and infrared images of AgNW and (Chi/Cell)$_{10}$@Al-AgNW TEs with different applied voltages, relative compositions of C–C, C=N, C–N, C–O, and C=O bonds and elemental composition analysis in AgNW and (Chi/Cell)$_n$@Al-AgNW TEs, FoM value of AgNW, (Chi/Cell)$_n$@Al-AgNW TEs, and TEs in other literature studies. See DOI: https://doi.org/10.1039/d4nh00285g

protective coating materials exhibit promise for improving the stability of AgNW-based transparent electrodes (TEs) and FTEs, there is still a strong demand to develop an efficient protection strategy to meet the overall requirements of a protective layer such as a simple coating process, high stability, gas barrier properties, film formability, transparency, flexibility, mechanical strength, and affinity to AgNWs and substrates.[38] In addition, the coating materials need to be eco-friendly and biorenewable, considering environmental sustainability.[39]

In this regard, chitin and cellulose are promising candidates because of their abundance in natural crustaceans and plants and their unique physicochemical properties, which can satisfy most requirements as protective materials.[40–42] Thus, chitin and cellulose nanofibers (Chi and Cell) have been extensively investigated as building blocks for gas barrier films in various packaging applications.[43] Chi and Cell are easily deposited onto arbitrary substrates through a layer-by-layer (LBL) assembly process based on their opposite surface charges, resulting in thin or free-standing films.[44,45] These LBL-assembled films exhibit excellent transparency, mechanical strength, flexibility, and gas barrier properties based on their stiff chain structures and low free volume attributed to the ionic cross-linking of amine and carboxylic acid groups from Chi and Cell, respectively.[46,47] Given these properties, it was expected that the LBL-assembled thin films of Chi and Cell could effectively protect the AgNW FTEs for flexible electronics.

Here, we developed a simple method to fabricate highly stable AgNW-based FTEs through the LBL assembly of Chi and Cell. Chi and Cell were alternately deposited on the aldehyde-modified AgNW (Al-AgNW) FTEs by a simple dip-coating process. Uniform and continuous thin films of Chi and Cell were successfully formed on Al-AgNW FTEs. The aldehyde modification and resultant thin film did not compromise the excellent optoelectrical properties of AgNW FTEs; rather, it improved the transmittance at 550 nm due to the reduced surface roughness of AgNW FTEs. The durability of AgNW and $(Chi/Cell)_n$ bilayers coated Al-AgNW ($(Chi/Cell)_n$@Al-AgNW) FTEs was systemically investigated against various harsh conditions (where n is the number of bilayers). $(Chi/Cell)_n$@Al-AgNW FTEs exhibited remarkable and comprehensive stability compared to pristine AgNW FTEs under UV/O_3 treatment, high temperatures, corrosive chemicals, sonication, and bending tests. Based on their excellent durability, $(Chi/Cell)_{10}$@Al-AgNW FTEs (10 is the optimized number of bilayers) were successfully employed as a transparent heater (TH) and pressure sensor, showing their compatibility with flexible electronics with high performance compared to pristine AgNW FTEs.

Experimental section

Materials

Silver nitrate, sodium chloride, glycerol, sodium bicarbonate, sodium hydroxide, ethanol, sodium sulfide, ammonium hydroxide (30%), hydrochloric acid (37%), hydrogen peroxide (30%), and sulfuric acid (98%) were purchased from Daejung Chemicals (Siheung, South Korea). Glutaraldehyde (25%) and poly(vinyl pyrrolidone) (PVP, M_W = 1 300 000) were purchased from Alfa Aesar (Ward Hill, Massachusetts, USA). Trichloro(1*H*,1*H*,2*H*,2*H*-tridecafluoro-*n*-octyl)silane (FOTS) was purchased from TCI (Tokyo, Japan). Chi (degree of deacetylation: >50%, pH 3.5) and Cell (TEMPO-mediated oxidized, pH 7.0) with an average diameter of 5 to 20 nm were purchased from ANPOLY (Pohang, South Korea). All chemicals were used as received without purification.

Fabrication of AgNW TEs and FTEs

AgNW was synthesized with our previously reported protocol.[39] 70 μL of the ethanolic suspension of AgNWs (5 mg mL^{-1}) was spin-coated onto cleaned glass or PET substrates with a dimension of 2.5 × 2.5 cm^2 at 1800 rpm. The glass substrates were cleaned through piranha treatment as described in our previous report.[48] The PET substrates were cleaned through sonication in water and ethanol for 5 min, respectively, and then treated with oxygen plasma for 15 min. The spin-coated AgNW on the glass and PET substrates were thermally treated at 180 °C for 1 min.

Fabrication of $(Chi/Cell)_n$@Al-AgNW TEs and FTEs

Chi and Cell were alternately deposited on AgNW TEs and FTEs through the LBL assembly process (glass and PET substrates were utilized for TEs and FTEs, respectively). Prior to the LBL assembly, the surfaces of AgNW TEs and FTEs were modified with aldehyde functional groups through the Claisen–Schmidt reaction.[39] Then, aqueous suspensions of Chi and Cell were prepared at a concentration of 0.4 wt% and adjusted to pH 3.5 and 7.0, respectively. Al-AgNW TEs and FTEs were immersed in the suspension of Chi for 1 h, washed with water and ethanol, and dried under a stream of N_2 gas. The resulting Chi-coated Al-AgNW (Chi@Al-AgNW) TEs and FTEs were then immersed in the suspension of Cell for 1 h, washed with water and ethanol, and dried under a stream of N_2 gas. These sequential LBL assembly cycles of Chi and Cell were defined as one LBL cycle, and this cycle was repeated until the desired number of $(Chi/Cell)_n$ bilayers was achieved. Finally, the resulting $(Chi/Cell)_n$@Al-AgNW TEs and FTEs were dried at 120 °C for 2 h under reduced pressure to remove any remaining water and ethanol.

Stability tests of AgNW and $(Chi/Cell)_n$@Al-AgNW TEs and FTEs

All stability tests were carried out by monitoring the electrical resistance changes of the TEs and FTEs using a two-point resistance measurement system. For the measurements, the silver paste was applied to the pair of edges facing each other on the AgNW and $(Chi/Cell)_n$@Al-AgNW TEs and FTEs and connected to a handheld digital multimeter (U1281A, Keysight Technologies, Inc.). The oxidation and optochemical stability were examined using a UV/O_3 cleaner with 184 and 254 nm UV light (model AC-3, AhTech LTS Co., Ltd). The thermal stability was explored using a hot plate. The AgNW and $(Chi/Cell)_n$@Al-AgNW TEs were placed on a hot plate and subjected to increasing temperatures from 100 to 350 °C at a ramping rate of 10 °C min^{-1}. A thermal stability test was also performed at a

fixed temperature of 250 °C. Chemical stability was investigated by dropping Na_2S (1%), HCl (10%), and NH_3 (30%) solutions onto the surface of the AgNW and $(Chi/Cell)_n$@Al-AgNW TEs and FTEs. The sonication test was carried out using an ultrasonic bath with water (Branson 2800, at a frequency of 40 kHz in the highest power mode). The bending test was performed using a 1-axis motion controller (STM-1-TS, ST1 Corp.) while measuring the electrical resistance change as a function of the bending radius. The 10 000 cycles of the bending test were additionally conducted with a fixed bending radius of 2.5 mm.

Fabrication of the pressure sensor

Polydimethylsiloxane (PDMS) was prepared by mixing the base and curing agents at a weight ratio of 10 : 1 (base to curing agent). The micropatterned Si mold was oxygen plasma-treated for 30 min and then subjected to vapor deposition of FOTS to facilitate the detachment of PDMS from the Si mold. The as-prepared PDMS precursor was spin-coated onto a micropatterned Si mold at 500 rpm for 1 min and then thermally treated at 100 °C for 6 h. The PDMS film was peeled off from the Si mold and inserted between the pair of AgNW and $(Chi/Cell)_{10}$@Al-AgNW FTEs.

Characterization

Transmittance spectra were obtained using a Varian Cary 50 Conc (Varian, Inc., USA). X-ray photoelectron spectroscopy (XPS) analysis was carried out using a Thermo Scientific K-alpha spectrometer (Thermo VG, USA) with monochromated Al Kα (1486.6 eV). Fourier transform infrared (FT-IR) analysis was carried out using FTIR-7600 (Lambda Scientific Systems, Inc., USA). The zeta potential values were acquired using a Zetasizer Nano ZS (Malvern, UK). Scanning electron microscopy (SEM) images were acquired using a JSM6700F microscope (JEOL, Japan). Atomic force microscopy (AFM) images were obtained using Multimode 8 (Bruker, USA). The sheet resistance was measured using a four-point probe instrument (M4P-302, MS-Tech, Korea). For evaluating the performance as a TH, a DC power supply (DP30-05U, Toyotech, Korea) was used to apply the voltage to the TEs. Then, the temperature change as a function of voltage was monitored using an IR camera (FLIR-E6390, FLIR Systems, Inc., Sweden). For evaluating the performance as a pressure sensor, the capacitance of the AgNW and $(Chi/Cell)_{10}$@Al-AgNW-based FTEs was measured using an impedance analyzer (IM 3570, HIOKI, Japan) while applying an AC voltage of 1 V at 1 MHz frequency. Pressure was applied using a universal testing machine (UTM) (ST-1000, SALT Co., Ltd, Korea) equipped with a 10 N load cell under a 2 mm min^{-1} loading rate.

Results and discussion

AgNW and $(Chi/Cell)_n$@Al-AgNW TEs and FTEs were fabricated using an all-solution process (Fig. 1a). First, the AgNW suspension

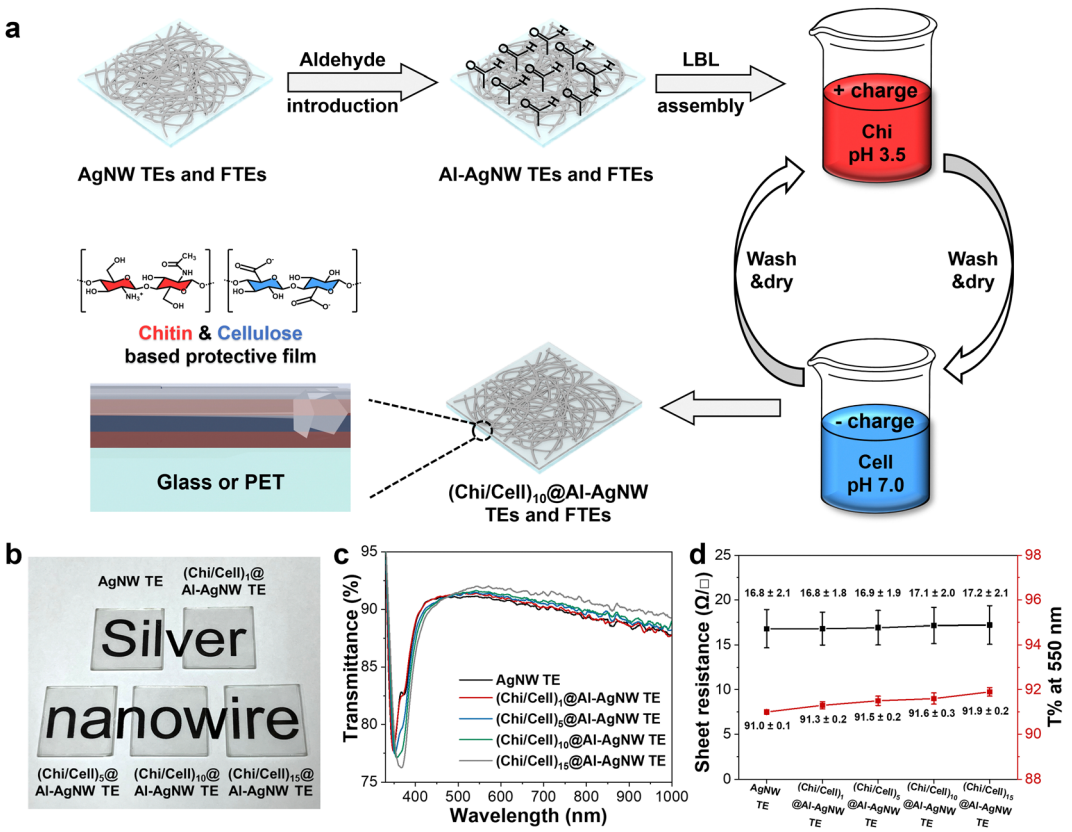

Fig. 1 (a) Schematic diagram for the fabrication of $(Chi/Cell)_n$@Al-AgNW TEs and FTEs. (b) Optical images, (c) transmittance spectra, and (d) sheet resistance and transmittance at 550 nm of AgNW, $(Chi/Cell)_1$, $(Chi/Cell)_5$, $(Chi/Cell)_{10}$, and $(Chi/Cell)_{15}$ @Al-AgNW TEs.

was spin-coated onto the glass or PET substrate to construct electrically conductive networks for TEs and FTEs, respectively (the characterization of AgNWs was provided in Fig. S1 and S2, ESI†). Second, the surface of the AgNW networks was modified with aldehyde functional groups to increase the deposition density of the first Chi layer and to afford chemical cross-linking of the AgNW networks through a Schiff base reaction with the amine groups of Chi. These effects were thoroughly confirmed in our previous report.[39] Third, the Chi and Cell were sequentially assembled on the Al-AgNW TEs and FTEs through a simple dip-coating method until the desired number of $(Chi/Cell)_n$ bilayers was achieved (the characterization of Chi and Cell was provided in Fig. S3, ESI†). Finally, the resulting TEs and FTEs were fully dried in a vacuum oven.

The LBL assembly was performed for up to 15 cycles, and the resulting $(Chi/Cell)_n$@Al-AgNW TEs were characterized by monitoring the optical images, transmittance spectra, and sheet resistance at 1, 5, 10, and 15 LBL assembly cycles. Their optical images showed that the transparency of the resulting TEs did not deteriorate even after 15 cycles of LBL assembly (Fig. 1b). The transmittance at 550 nm gradually increased from 91.0 to 91.9% after 15 cycles of LBL assembly (Fig. 1c and d). These results were obtained because the $(Chi/Cell)_n$ bilayers reduced the light scattering generated from the rough surface of the AgNW TEs. Light scattering generally takes place between air and the surface of the AgNW TEs due to the nanoscale diameter of the AgNWs and the nanostructured gaps in the AgNW networks.[34] The $(Chi/Cell)_n$ bilayers gradually covered the rough surface of the AgNW networks, and thus, the $(Chi/Cell)_n$@Al-AgNW TEs have a smoother surface than the AgNW TEs as the LBL assembly progressed, leading to a decrease in light scattering. Additionally, the transverse plasmon resonance (TPR) peak of AgNW TEs was red-shifted from 348 to 367 nm after the 15 cycles of LBL assembly, accompanied by a decrease in transmittance (Fig. 1c). This shift also indicated that the $(Chi/Cell)_n$ bilayers were successfully deposited on the surface of the AgNW networks during the LBL assembly cycles.[39] Furthermore, the sheet resistance of the AgNW TEs remained almost constant without notable changes in the AgNW diameter, even after 15 cycles of LBL assembly (Fig. 1d and Fig. S4, ESI†). All these results clearly suggested that the LBL assembly process did not degrade the optoelectrical properties of AgNW TEs.

To confirm the formation of $(Chi/Cell)_n$ bilayers on AgNW TEs, the surface morphology and chemical compositions of AgNW and $(Chi/Cell)_n$@Al-AgNW TEs were investigated using SEM, AFM, and XPS. SEM images revealed that fibrous structures were gradually deposited on the surface of the AgNW TEs with LBL assembly cycles (Fig. 2). After 10 cycles of LBL assembly, a uniform and continuous thin film was formed on the AgNW TEs, indicating that the overall surface of the AgNW TEs was covered after 10 cycles of the LBL assembly (Fig. 2). AFM images also showed that fibrous structures were gradually deposited on the AgNW TEs during the LBL assembly cycles. Subsequently, the root-mean-square roughness (R_q) of the AgNW TEs decreased from 28.3 to 16.6 nm after 15 cycles of LBL assembly (Fig. 2). These findings suggested that $(Chi/Cell)_n$@Al-AgNW TEs have a relatively smooth surface compared to pristine AgNW TEs, which correlates with the increase in transmittance at 550 nm during the LBL assembly cycles. Moreover, R_q was also measured where AgNW networks

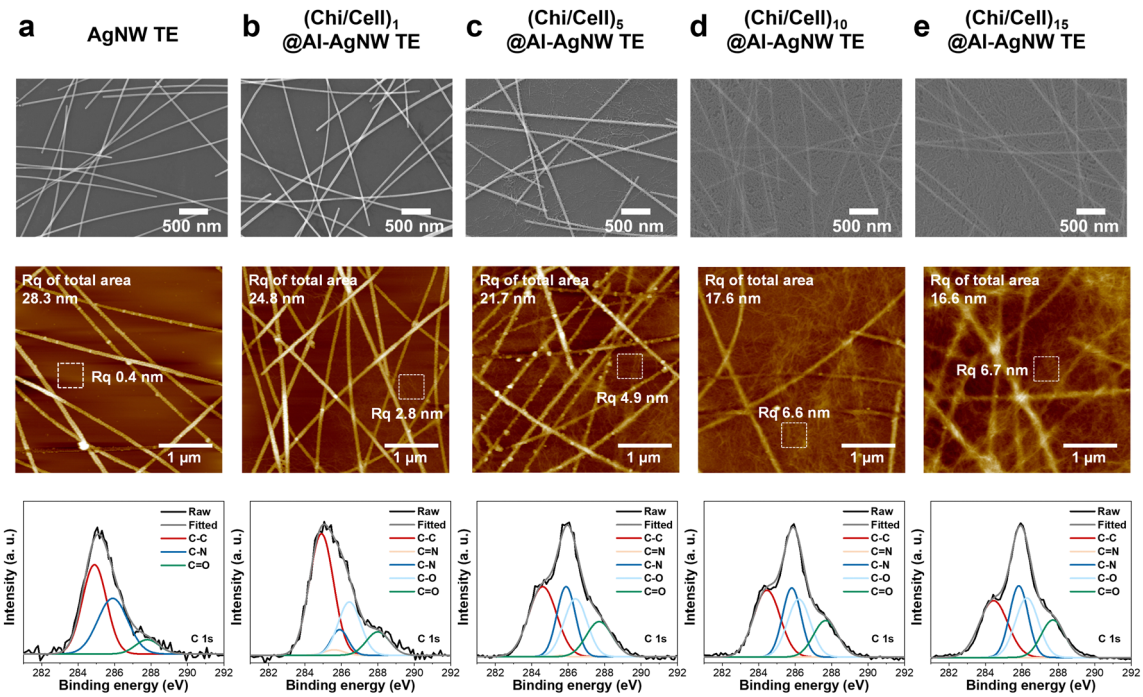

Fig. 2 SEM images, AFM images, R_q of total and squared areas, and C 1s XPS spectra of (a) AgNW, (b) $(Chi/Cell)_1$, (c) $(Chi/Cell)_5$, (d) $(Chi/Cell)_{10}$, and (e) $(Chi/Cell)_{15}$@Al-AgNW TEs.

did not exist (at a surface area of 0.4 μm^2). R_q gradually increased from 0.4 to 6.6 nm with 10 cycles of LBL assembly, and this increase was almost saturated after 10 cycles (Fig. 2). These results also corroborated that the $(Chi/Cell)_n$ bilayers almost covered the overall surface of the AgNW TEs after 10 cycles of LBL assembly.[39] In XPS analysis, the C 1s XPS spectrum of the AgNW TEs was deconvoluted to 284.9, 285.9, and 287.8 eV corresponding to C–C, C–N, and C═O bonds with relative compositions of 51.8, 40.2, and 8.0%, respectively. After the introduction of the aldehyde functional groups, the relative composition of C═O bonds notably increased to 18.7% (Fig. 2 and Table S1, ESI†).[39] Then, the C 1s XPS spectrum of Chi@Al-AgNW TEs showed new peaks at 286.5 and 285.6 eV corresponding to C–O and C═N bonds derived from the deposited Chi and its imine linkage with the aldehyde groups of Al-AgNW, respectively (Fig. S5 and Table S1, ESI†). In the $(Chi/Cell)_1$@Al-AgNW TEs, the relative compositions of C═N and C–N bonds decreased with an increase of C–O bonds (C═N bonds: from 2.9 to 2.1%, C–N bonds: from 11.4 to 8.4%, and C–O bonds: from 16.0 to 23.0%), indicating that Cell was successfully deposited on the Chi@Al-AgNW TEs (Fig. 2 and Table S1, ESI†). After 5 cycles of LBL assembly, the relative composition of C═N bonds decreased to 0.2%, with an increase of C–N bonds to 23.6%. With further LBL assembly over 10 cycles, the C═N bonds were not observed with a constant signal of C–N and C–O bonds (Fig. 2 and Table S1, ESI†). Moreover, the atomic percentage of Ag was gradually diminished during the LBL assembly, and it was also not detected after 10 cycles of LBL assembly (Table S2, ESI†). Importantly, the C═N bonds and Ag elements only existed at the bottom layer of $(Chi/Cell)_n$@Al-AgNW TEs.[39] Considering this point, it clearly supported that the surface of AgNW TEs was entirely covered with $(Chi/Cell)_n$ bilayers after 10 cycles of the LBL assembly.

The protective ability of the $(Chi/Cell)_n$ bilayers on AgNW TEs was investigated under various harsh conditions. First, AgNW and $(Chi/Cell)_n$@Al-AgNW TEs were treated with UV/O_3 cleaner to explore their oxidation and optochemical stability. Electrical failure of the AgNW TEs occurred within 20 min, whereas the $(Chi/Cell)_1$ and $(Chi/Cell)_5$@Al-AgNW TEs did not exhibit electrical failure for 25 and 35 min, respectively (Fig. 3a). After 10 cycles of LBL assembly, the electrical conductivity of the $(Chi/Cell)_n$@Al-AgNW TEs was almost maintained until 40 min and gradually increased after 45 min (Fig. 3a). Additionally, their SEM images showed that the AgNW networks of the AgNW TEs were fragmented after UV/O_3 treatment for 30 min, but the morphology of the $(Chi/Cell)_{10}$@Al-AgNW TEs was intact under the equal conditions (Fig. S6a and b, ESI†). These results corroborated that the $(Chi/Cell)_n$ bilayers successfully protected the AgNW TEs under highly oxidative conditions. Second, the thermal stability of the AgNW and $(Chi/Cell)_n$@Al-AgNW TEs was examined on a hot plate with increasing temperatures up to 350 °C at a ramping rate of 10 °C min^{-1}. The temperature corresponding to R/R_0 = 10 was defined as the thermal degradation temperature (T_D). The T_D of the AgNW TEs gradually increased from 270 to 300 °C with 5 cycles of LBL assembly, and it further increased to 340 °C with over 10 cycles of LBL assembly (Fig. 3b). These results also suggested that $(Chi/Cell)_n$ bilayers could improve the thermal stability of AgNW TEs. Moreover, the thermal stability of the AgNW and $(Chi/Cell)_{10}$@Al-AgNW TEs was examined at a

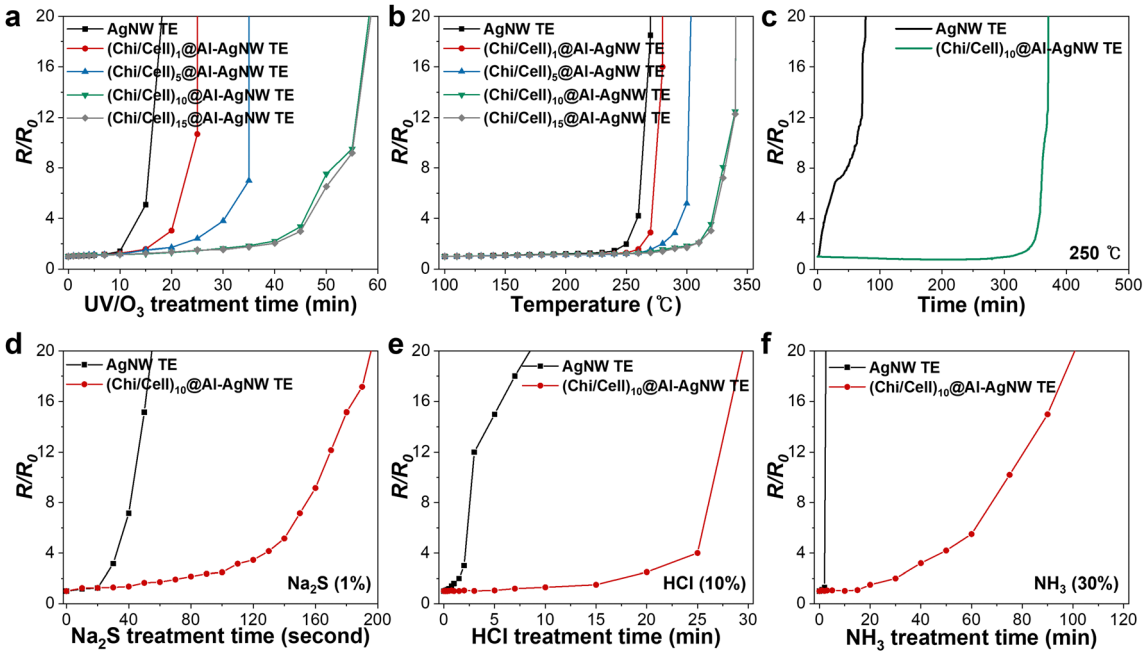

Fig. 3 Relative variation in the electrical resistance of AgNW, $(Chi/Cell)_1$, $(Chi/Cell)_5$, $(Chi/Cell)_{10}$, and $(Chi/Cell)_{15}$ @Al-AgNW TEs as a function of (a) UV/O_3 treatment time and (b) temperature (100 to 350 °C at a ramping rate of 10 °C min^{-1}). (c) Relative variation in the electrical resistance of AgNW and $(Chi/Cell)_{10}$@Al-AgNW TEs at 250 °C as a function of time. Relative variation in the electrical resistance of AgNW and $(Chi/Cell)_{10}$@Al-AgNW TEs as a function of time with treatments of (d) Na_2S (1%), (e) HCl (10%), and (f) NH_3 (30%) solutions.

constant temperature of 250 °C. The electrical conductivity of the AgNW TEs drastically deteriorated, and electrical failure was observed after 60 min. However, that of the $(Chi/Cell)_{10}$@Al-AgNW TEs was almost maintained up to 350 min, and electrical failure was observed after 360 min (Fig. 3c). The SEM images also showed that the AgNW networks were fragmented into small particles after thermal treatment for 300 min, but the morphology of the $(Chi/Cell)_{10}$@Al-AgNW TEs was almost maintained after the equal treatment (Fig. S6c and d, ESI†). The fragmentation of AgNW TEs was attributed to Rayleigh instability, which leads to the breaking of AgNWs into small particles, ultimately destroying the percolation of AgNW networks.[37,39] All these results supported that the stability enhancement of AgNW TEs was saturated after 10 cycles of LBL assembly. This finding is consistent with the results of SEM, AFM, and XPS analyses, suggesting that the surface of the AgNW TEs was fully covered after 10 cycles of LBL assembly. The chemical stability of the AgNW and $(Chi/Cell)_{10}$@Al-AgNW TEs was also examined by dropping 200 μL of Na_2S (1%), HCl (10%), and NH_3 (30%) solutions on the TEs, as depicted in Fig. S7 (ESI†). The AgNW TEs exhibited electrical failure after 1, 10, and 3 min in Na_2S (1%), HCl (10%), and NH_3 (30%) solutions, respectively. However, electrical failure occurred on the $(Chi/Cell)_{10}$@Al-AgNW TEs after 3, 30, and 105 min under the equal treatments (Fig. 3d–f). These results also showed that the $(Chi/Cell)_{10}$ bilayers could greatly improve the stability of AgNW TEs against various reactive chemicals including sulfides, acids, and bases.

Based on their high thermal and oxidation stability, $(Chi/Cell)_{10}$@Al-AgNW TEs were utilized as TH, which is an essential component in various fields of thermal management. The surface temperatures of the AgNW TEs reached 34, 56, 90, and 133 °C at 2, 4, 6, and 8 V, respectively. However, electrical failure was observed at 165 °C when 10 V was applied. In contrast, the $(Chi/Cell)_{10}$@Al-AgNW TEs exhibited a stable heating performance of 174 °C at 10 V (Fig. 4a–c). Importantly, the electrical heating behaviors and hot spots of the AgNW TEs were similar to those of the $(Chi/Cell)_{10}$@Al-AgNW TEs up to 8 V (Fig. S8 and S9, ESI†). When 10 V was applied, the hot spots of the AgNW TEs were separated owing to electrical failure, but the $(Chi/Cell)_{10}$@Al-AgNW TEs exhibited relatively homogeneous and broad hot spots (Fig. 4d). Additionally, the SEM images of the AgNW TEs showed that the AgNW networks of the AgNW TEs were disconnected at their junction points after applying 10 V for 5 min, whereas those of the $(Chi/Cell)_{10}$@Al-AgNW TEs were intact under the equal treatments (Fig. S10, ESI†). The response to the applied voltages was further explored by ramping the voltages up and down and repeating on (3 min) and off (4 min) at 8 V. The surface temperature of the $(Chi/Cell)_{10}$@Al-AgNW TEs rapidly increased and decreased with varying applied voltages from 0 to 10 V and 10 to 0 V. The temperature was identical at the equally applied voltages regardless of the ramping of the voltages up and down. However, electrical failure occurred in the AgNW TEs at 10 V after reaching 165 °C (Fig. 4e). Subsequently, a repeating test was performed for 15 cycles. The $(Chi/Cell)_{10}$@Al-AgNW TEs showed a steady and stable heating performance for 15 cycles of the repeating test, whereas the surface temperature of the AgNW TEs gradually decreased under the equal conditions of the repeating test (Fig. 4f). Moreover, the duration of heating performance was also tested at a constant voltage of 8 V. The surface temperature of the AgNW TEs reached 133 °C after 3 min, but it drastically decreased after 10 min. In stark contrast, the temperature of the $(Chi/Cell)_{10}$@Al-AgNW TEs was stably maintained for 180 min and gradually decreased (Fig. 4g). All these results clearly confirmed that the $(Chi/Cell)_{10}$ bilayers improved the durability and performance of the AgNW TEs as a TH device.

The mechanical stability of FTEs is also an important factor in pressure sensors, where mechanical stress should be

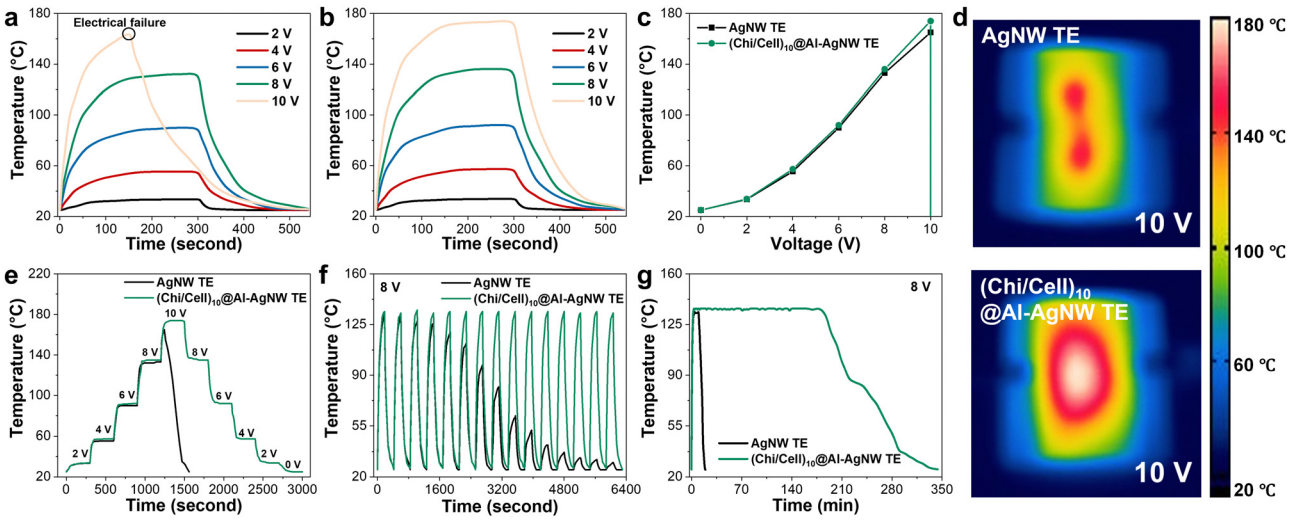

Fig. 4 Temperature profiles of the (a) AgNW and (b) $(Chi/Cell)_{10}$@Al-AgNW TEs as a function of times at different DC voltages. (c) Temperature versus voltage graphs of the AgNW and $(Chi/Cell)_{10}$@Al-AgNW TEs. (d) Infrared images of AgNW and $(Chi/Cell)_{10}$@Al-AgNW TEs by applying 10 V. Temperature profiles of the AgNW and $(Chi/Cell)_{10}$@Al-AgNW TEs as a function of time with (e) varying applied voltages, (f) repeated heating 15 times, and (g) at a constant voltage of 8 V.

applied. Therefore, the mechanical stability of the AgNW and $(Chi/Cell)_{10}$@Al-AgNW FTEs was explored through sonication and bending tests. First, the FTEs were sonicated in a water bath, and their electrical resistance changes were monitored. The electrical failure of the AgNW FTEs occurred after 15 min, but the resistance and transmittance of $(Chi/Cell)_{10}$@Al-AgNW FTEs only slightly increased, even after 300 min of sonication (Fig. 5a and b). Second, the AgNW and $(Chi/Cell)_{10}$@Al-AgNW FTEs were bent while monitoring the change in the electrical resistance as a function of the bending radius. The resistance of the AgNW FTEs increased 1.2-fold when the bending radius decreased from 25 to 2.5 mm (Fig. 5c). This increase was due to the slipping and delamination of the AgNW at the junction points while bending was applied.[31] In marked contrast, the $(Chi/Cell)_{10}$@Al-AgNW FTEs showed a negligible change in the electrical resistance, even after decreasing the bending radius to 2.5 mm (Fig. 5c). Furthermore, the 10 000 cycles of the bending test were performed with a fixed bending radius of 2.5 mm. The electrical resistance of the AgNW TEs sharply increased by 1.8-fold for 530 cycles and then gradually increased by 2.3-fold for 10 000 cycles. On the other hand, the resistance of the $(Chi/Cell)_{10}$@Al-AgNW FTEs only slightly increased by 1.3-fold for 10 000 cycles (Fig. 5d). All these results indicated that $(Chi/Cell)_{10}$ bilayers improve not only the oxidation, thermal, and chemical stability of the AgNW networks but also their mechanical stability.

Encouraged by its excellent mechanical stability and flexibility, $(Chi/Cell)_{10}$@Al-AgNW FTEs were applied to a capacitive-type transparent pressure sensor, which requires high stability against repeated mechanical agitation. A PDMS elastomer was inserted between the $(Chi/Cell)_{10}$@Al-AgNW FTEs and assembled, as depicted in the inset of Fig. 6a. The PDMS elastomer has a micropatterned pyramidal topology with an edge-to-edge distance and height of 50 μm and a bottom area of 50 × 50 μm^2, respectively (Fig. 6a). The capacitance change ($\Delta C/C_0$) and sensitivity were monitored as a function of applied pressure up to 25 kPa. Sensitivity is defined as the initial slope of the capacitance change *versus* the pressure graph.[49] As a result, the pressure sensor composed of $(Chi/Cell)_{10}$@Al-AgNW FTEs showed more significant capacitance change against the applied pressure with higher sensitivity than that of the pressure sensor composed of AgNW FTEs (the pressure sensitivity of AgNW and $(Chi/Cell)_{10}$@Al-AgNW FTEs were 0.52 and 1.85 kPa^{-1}, respectively.) (Fig. 6b). This enhanced sensitivity was attributed to the lower C_0 value of the sensor composed of $(Chi/Cell)_{10}$@Al-AgNW FTEs compared to that of the sensor composed of AgNW FTEs resulting from the presence of $(Chi/Cell)_{10}$ bilayers.[50] In addition, the $(Chi/Cell)_{10}$@Al-AgNW FTEs-based pressure sensor exhibited more sensitive responses than the AgNW FTEs-based pressure sensor against gentle touch with a finger (Fig. 6c). Finally, the durability of the $(Chi/Cell)_{10}$@Al-AgNW FTEs-based pressure sensor was evaluated by repeated loading and unloading at a fixed pressure of 2.5 kPa for 5000 cycles. The capacitance change gradually decreased for 1500 cycles in the AgNW FTEs-based pressure sensor, but it was stably maintained on the $(Chi/Cell)_{10}$@Al-AgNW FTEs-based pressure sensor for 5000 cycles (Fig. 6d). Taken together, all of these results confirmed that $(Chi/Cell)_{10}$@Al-AgNW FTEs are a more effective and durable component than AgNW FTEs for the fabrication of a capacitive-type transparent pressure sensor.

Finally, the performance of the $(Chi/Cell)_n$@Al-AgNW TEs was quantitatively compared using the figure of merit (FoM)

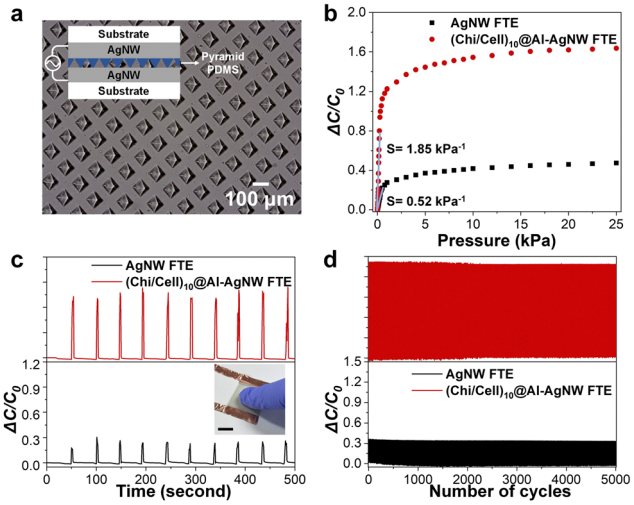

Fig. 6 (a) Optical image of the micropatterned PDMS elastomer inserted between FTEs. The inset in (a) shows the schematic of the pressure sensor. (b) Relative capacitance change ($\Delta C/C_0$) and sensitivity of pressure sensors composed of AgNW and $(Chi/Cell)_{10}$@Al-AgNW FTEs as a function of pressure. Relative capacitance change ($\Delta C/C_0$) of the pressure sensors composed of AgNW and $(Chi/Cell)_{10}$@Al-AgNW FTEs as a function of time with (c) gentle finger touch and (d) repeated loading–unloading cycles at a fixed pressure of 2.5 kPa. The inset in (c) shows the photograph of a gentle finger touch, and the scale bar represents 1 cm.

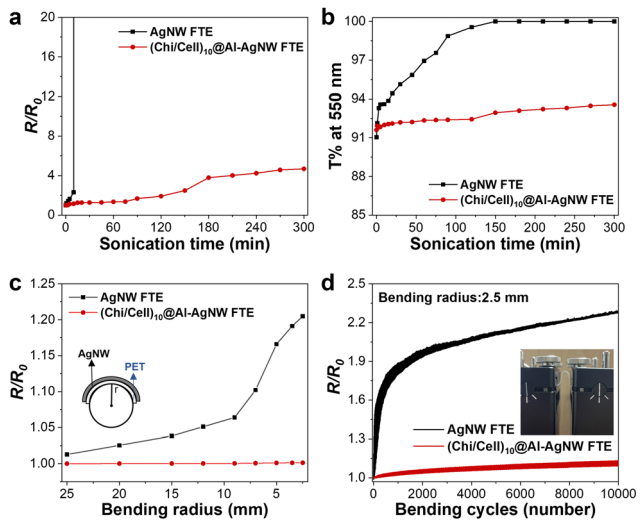

Fig. 5 (a) Relative variation in the electrical resistance and (b) transmittance at 550 nm of AgNW and $(Chi/Cell)_{10}$@Al-AgNW FTEs as a function of sonication time. Relative variation in the electrical resistance of AgNW and $(Chi/Cell)_{10}$@Al-AgNW FTEs as a function of (c) the bending radius and (d) bending cycles at a fixed bending radius of 2.5 mm.

calculated by the following equation:

$$\frac{\sigma_{DC}}{\sigma_{OP}(\lambda)} = \frac{188.5}{R_s}\left(\frac{1}{\frac{1}{\sqrt{T(\lambda)}} - 1}\right)$$

Here, $\sigma_{DC}/\sigma_{OP}(\lambda)$ is the standard value for the FoM of TEs, and σ_{DC}, $\sigma_{OP}(\lambda)$, $T(\lambda)$, and R_s are the DC conductivity, optical conductivity, transmittance at λ nm, and sheet resistance, respectively.[39] The FoM value of AgNW TEs gradually increased from 232 to 254 after 15 cycles of LBL assembly due to the gradual increase in the transmittance at 550 nm and the negligible change in the sheet resistance during the LBL assembly process. These values significantly surpassed the minimum requirement for industrial applications (35) and were comparable to previously reported TEs (the FoM values of AgNW, $(Chi/Cell)_n$@Al-AgNW, and other TEs are provided in Table S3, ESI†). These results demonstrated the strong potential of the $(Chi/Cell)_{10}$@Al-AgNW TEs for practical applications in various industries.

Conclusions

We demonstrated an efficient and sustainable protection strategy for fabricating highly durable AgNW-based FTEs. Biorenewable Chi and Cell presenting opposite surface charges were successively deposited on the AgNW FTEs up to 15 cycles of LBL assembly. The resulting $(Chi/Cell)_n$ bilayers did not deteriorate the excellent optoelectrical properties of the AgNW FTEs but enhanced their stability against various agitations. The stability enhancement reached a plateau after 10 LBL assembly cycles, forming an integrative layer, as confirmed by SEM, AFM, and XPS analyses. In particular, the optimized $(Chi/Cell)_{10}$@Al-AgNW FTEs exhibited comprehensive stability under UV/O_3 treatment for 40 min, high temperature at 250 °C for 350 min, Na_2S (1%), HCl (10%), and NH_3 (30%) treatments for 3, 30, and 105 min, respectively, sonication for 300 min, and 10 000 cycles of bending test. Furthermore, $(Chi/Cell)_{10}$@Al-AgNW FTEs showed great potential as durable and high-performance THs and pressure sensors. Consequently, this study provides a sustainable and effective approach for developing highly durable AgNW-based FTEs, and we believe that this strategy significantly extends their applicability to flexible electronics.

Author contributions

Yoo-Bin Kwon: conceptualization, data curation, investigation, methodology, formal analysis, validation, visualization, writing – original draft, and writing – review & editing. Seongwon Cho: data curation, investigation, and methodology. Dal-Hee Min: funding acquisition, supervision, and writing – review & editing. Young-Kwan Kim: conceptualization, data curation, methodology, formal analysis, investigation, funding acquisition, supervision, writing – original draft, and writing – review & editing.

Data availability

The data supporting this article have been included as part of the ESI.†

Conflicts of interest

There are no conflicts to declare.

Acknowledgements

This work was supported by the National Research Foundation of Korea (NRF) grant funded by the Korean government, Ministry of Science and ICT (MSIT) (No. 2022R1C1C1008388 and 2021R1A2B5B03086506). This research was also supported by the Basic Science Research Program through the National Research Foundation of Korea (NRF) funded by the Ministry of Education (2022R1A6A1A03053343). Some images used for the graphical abstract were downloaded from Pixabay. We thank Pixabay for providing the free images.

References

1 H. Wu, D. Kong, Z. Ruan, P. C. Hsu, S. Wang, Z. Yu, T. J. Carney, L. Hu, S. Fan and Y. Cui, *Nat. Nanotechnol.*, 2013, **8**, 421–425.
2 H. Kang, S. Jung, S. Jeong, G. Kim and K. Lee, *Nat. Commun.*, 2015, **6**, 6503.
3 Y. Sun, M. Chang, L. Meng, X. Wan, H. Gao, Y. Zhang, K. Zhao, Z. Sun, C. Li, S. Liu, H. Wang, J. Liang and Y. Chen, *Nat. Electron.*, 2019, **2**, 513–520.
4 H. B. Lee, W. Y. Jin, M. M. Ovhal, N. Kumar and J. W. Kang, *J. Mater. Chem. C*, 2019, **7**, 1087–1110.
5 X. Fan, *Adv. Funct. Mater.*, 2021, **31**, 2009399.
6 V. H. Nguyen, D. T. Papanastasiou, J. Resende, L. Bardet, T. Sannicolo, C. Jiménez, D. Muñoz-Rojas, N. D. Nguyen and D. Bellet, *Small*, 2022, **18**, 2106006.
7 X. Zeng, Y. Ding, X. Yuan, C. Jiang, Y. Wang, Y. Song, Y. Li, B. Shao, Y. Wang and B. Sun, *Adv. Funct. Mater.*, 2024, **34**, 2309730.
8 W. J. Yu, S. H. Chae, S. Y. Lee, D. L. Duong and Y. H. Lee, *Adv. Mater.*, 2011, **23**, 1889–1893.
9 K. A. Nirmal, W. Ren, A. C. Khot, D. Y. Kang, T. D. Dongale and T. G. Kim, *Adv. Sci.*, 2023, **10**, 2300433.
10 H. J. Lee, B. H. Kim, A. V. Takaloo, K. R. Son, T. D. Dongale, K. M. Lim and T. G. Kim, *Adv. Opt. Mater.*, 2021, **9**, 2002010.
11 Y. Wang, W. Huang, Z. Zhang, L. Fan, Q. Huang, J. Wang, Y. Zhang and M. Zhang, *Nanoscale*, 2021, **13**, 11360–11369.
12 K. Ellmer, *Nat. Photonics*, 2012, **6**, 809–817.
13 S. Ye, A. R. Rathmell, Z. Chen, I. E. Stewart and B. J. Wiley, *Adv. Mater.*, 2014, **26**, 6670–6687.
14 K. W. Seo, J. Lee, J. Jo, C. Cho and J. Y. Lee, *Adv. Mater.*, 2019, **31**, 1902447.
15 D. S. Hecht, L. Hu and G. Irvin, *Adv. Mater.*, 2011, **23**, 1482–1513.

16 M. S. Lee, K. Lee, S. Y. Kim, H. Lee, J. Park, K. H. Choi, H. K. Kim, D. G. Kim, D. Y. Lee, S. Nam and J. U. Park, *Nano Lett.*, 2013, **13**, 2814–2821.
17 T. Sannicolo, M. Lagrange, A. Cabos, C. Celle, J. P. Simonato and D. Bellet, *Small*, 2016, **12**, 6052–6075.
18 A. I. Hofmann, E. Cloutet and G. Hadziioannou, *Adv. Electron. Mater.*, 2018, **4**, 1700412.
19 C. F. Guo and Z. Ren, *Mater. Today*, 2015, **18**, 143–154.
20 K. Zilberberg and T. Riedl, *J. Mater. Chem. A*, 2016, **4**, 14481–14508.
21 J. Kwon, Y. D. Suh, J. Lee, P. Lee, S. Han, S. Hong, J. Yeo, H. Lee and S. H. Ko, *J. Mater. Chem. C*, 2018, **6**, 7445–7461.
22 H. K. Park, D. Lee, H. Lee and S. Hong, *Mater. Horiz.*, 2020, **7**, 1387–1396.
23 M. R. Azani, A. Hassanpour and T. Torres, *Adv. Energy Mater.*, 2020, **10**, 2002536.
24 J. J. Patil, W. H. Chae, A. Trebach, K. J. Carter, E. Lee, T. Sannicolo and J. C. Grossman, *Adv. Mater.*, 2021, **33**, 2004356.
25 C. Ma, Y. F. Liu, Y. G. Bi, X. L. Zhang, D. Yin, J. Feng and H. B. Sun, *Nanoscale*, 2021, **13**, 12423–12437.
26 W. H. Chae, J. J. Patil and J. C. Grossman, *ACS Appl. Mater. Interfaces*, 2022, **14**, 34997–35009.
27 W. H. Chae, T. Sannicolo and J. C. Grossman, *ACS Appl. Mater. Interfaces*, 2020, **12**, 17909–17920.
28 S. R. Das, Q. Nian, M. Saei, S. Jin, D. Back, P. Kumar, D. B. Janes, M. A. Alam and G. J. Cheng, *ACS Nano*, 2015, **9**, 11121–11133.
29 H. Luo, H. Zhu, A. Di Ayingmo, Y. Zhang and L. Yu, *Mater. Sci. Eng. B*, 2024, **303**, 117304.
30 A. Khan, B. Faceira, L. Bardet, C. Sanchez-Velasquez, S. S. Nayak, C. Jiménez, D. Muñoz-Rojas, A. Rougier and D. Bellet, *ACS Appl. Mater. Interfaces*, 2024, **16**, 10439–10449.
31 S. Yu, X. Liu, M. Wu, H. Dong, X. Wang and L. Li, *ACS Appl. Mater. Interfaces*, 2021, **13**, 14470–14478.
32 Y. Qin, L. Yao, F. Zhang, R. Li, Y. Chen, Y. Chen, T. Cheng, W. Lai, B. Mi, X. Zhang and W. Huang, *ACS Appl. Mater. Interfaces*, 2022, **14**, 38021–38030.
33 C. Ma, X. M. Gao, Y. G. Bi, X. L. Zhang, D. Yin, X. M. Wen, Y. F. Liu, J. Feng and H. B. Sun, *Org. Electron.*, 2020, **84**, 105727.
34 Y. Jin, K. Wang, Y. Cheng, Q. Pei, Y. Xu and F. Xiao, *ACS Appl. Mater. Interfaces*, 2017, **9**, 4733–4741.
35 J. Ma, J. H. Kim, G. H. Lee, S. Jo and C. S. Kim, *J. Electron. Mater.*, 2021, **50**, 4908–4914.
36 A. Madeira, M. Plissonneau, L. Servant, I. A. Goldthorpe and M. Tréguer-Delapierre, *Nanomaterials*, 2019, **9**, 13–16.
37 G. S. Liu, Y. Xu, Y. Kong, L. Wang, J. Wang, X. Xie, Y. Luo and B. R. Yang, *ACS Appl. Mater. Interfaces*, 2018, **10**, 37699–37708.
38 X. Duan, Y. Ding and R. Liu, *Mater. Today Energy*, 2023, **37**, 101409.
39 Y. B. Kwon, J. H. Kim and Y. K. Kim, *ACS Appl. Mater. Interfaces*, 2022, **14**, 25993–26003.
40 M. Kostag and O. A. El Seoud, *Carbohydr. Polym. Technol. Appl.*, 2021, **2**, 100079.
41 S. K. Thomas, J. Parameswaranpillai, S. Krishnasamy, P. M. S. Begum, D. Nandi, S. Siengchin, J. J. George, N. Hameed, N. V. Salim and N. Sienkiewicz, *Carbohydr. Polym. Technol. Appl.*, 2021, **2**, 100095.
42 H. P. S. Abdul Khalil, C. K. Saurabh, A. S. Adnan, M. R. Nurul Fazita, M. I. Syakir, Y. Davoudpour, M. Rafatullah, C. K. Abdullah, M. K. M. Haafiz and R. Dungani, *Carbohydr. Polym.*, 2016, **150**, 216–226.
43 Z. Yu, Y. Ji, V. Bourg, M. Bilgen and J. C. Meredith, *Emergent Mater.*, 2020, **3**, 919–936.
44 T. Kim, T. H. Tran, S. Y. Hwang, J. Park, D. X. Oh and B. S. Kim, *ACS Nano*, 2019, **13**, 3796–3805.
45 Y. Ji, D. E. Shen, Y. Lu, G. T. Schueneman, M. L. Shofner and J. C. Meredith, *ACS Sustainable Chem. Eng.*, 2023, **11**, 10874–10883.
46 J. Wu, K. Zhang, N. Girouard and J. C. Meredith, *Biomacromolecules*, 2014, **15**, 4614–4620.
47 B. Duan, C. Chang, B. Ding, J. Cai, M. Xu, S. Feng, J. Ren, X. Shi, Y. Du and L. Zhang, *J. Mater. Chem. A*, 2013, **1**, 1867–1874.
48 Y. B. Kwon, S. Y. Cho, H. Jang, J. H. Kim and Y. K. Kim, *Langmuir*, 2021, **37**, 14205–14213.
49 K. H. Ha, H. Huh, Z. Li and N. Lu, *ACS Nano*, 2022, **16**, 3442–3448.
50 S. Lee, E. H. Kim, S. Yu, H. Kim, C. Park, S. W. Lee, H. Han, W. Jin, K. Lee, C. E. Lee, J. Jang, C. M. Koo and C. Park, *ACS Nano*, 2021, **15**, 8940–8952.